AIMS Materials Science, 9(4): 642–652.
DOI: 10.3934/matersci.2022039
Received: 08 April 2022
Revised: 13 June 2022
Accepted: 04 July 2022
Published: 16 August 2022

http://www.aimspress.com/journal/Materials

Research article

Agglomeration and dissolution of iron oxide nanoparticles in simplest biological media

Anna Godymchuk[1,*], Alexey Ilyashenko[2], Yury Konyukhov[3], Peter Ogbuna Offor[4] and Galiya Baisalova[5]

[1] Department of Material Science, Tomsk Polytechnic University, 30 Lenina avenue, 634050, Tomsk, Russia
[2] Joint-Stock Company "Scientific and Industrial Centre Polyus", 56V Kirova Avenue, 634050, Tomsk, Russia
[3] Department of Functional Nanosystems and High Temperature Materials, National University of Science and Technology "MISiS", 4 Leninsky avenue, 119049, Moscow, Russia
[4] Metallurgical and Materials Engineering Department, Africa Centre of Excellence for Sustainable Power and Energy Development (ACE-SPED), University of Nigeria, 410001, Nsukka, Nigeria
[5] Department of Chemistry, L.N. Gumilyov Eurasian National University, 2 Satpayev Street, 010008, Astana, Kazakhstan

* **Correspondence:** Email: godymchuk@tpu.ru.

Abstract: Despite high medical and biological potential, the penetration of iron oxide nanoparticles (NPs) into a human body can cause their dissolution with subsequent accumulation of highly toxic iron compounds. The paper describes the agglomeration and dissolution behavior of differently sized α-Fe_2O_3 NPs in the simplest biological solutions. The average sizes of the initial NPs according to the BET analysis are 12, 32, and 115 nm. Within 30–60 min exposure, the particle size and concentration of iron released into the solutions increases in the suspensions, accompanied by an intensive change of NPs surface charge. After an hour of exposure, the colloidal properties do not change significantly, although the dissolution degree ambiguously fluctuates. It has been shown that the agglomeration of the particles in the simplest pulmonary fluid is lower than in the simplest sweat fluid, compared to the dissolution degree, which is much higher in the pulmonary fluid than in the sweat. The colloidal stability of suspensions reduces with a decrease of NPs' size, e.g., the average size of particles is 315, 289, and 248 nm, while zeta potential is 2, 9, and 17 mV, respectively for 12, 32, and 115 nm NPs in 3-hour suspensions. It has been found that 24 h dissolution degree of α-Fe_2O_3

NPs reaches 2.3% and 0.4%, respectively, in the simplest pulmonary and sweat fluids. The mechanism of dissolution of hematite NPs in the slightly acidic and acidic mediums is proposed.

Keywords: iron oxide nanoparticles; agglomeration; dissolution; simplest sweat fluid; simplest pulmonary fluid

1. Introduction

Iron oxide nanoparticles (NPs) have found wide application in medicine [1] and biotechnology [2,3], and their intensive production [4] creates the conditions for NPs penetration into the human body. NPs can partially dissolve and undergo agglomeration in biological media. These effects were found even for NPs of chemically inert γ-Al_2O_3 [5]. Despite high medical and biological potential, the penetration of iron oxide NPs into the human body can cause their dissolution with subsequent accumulation of highly toxic iron compounds. Therefore, the dissolution and agglomeration of iron-containing NPs in biological fluids are of great issue.

The agglomeration of iron oxide NPs is actively studied in the literature [6–8]. However, little attention is paid to the solubility of iron-containing NPs in aqueous solutions [9] compared to colloidal particles γ-FeOOH [10], oxalate-coated α-Fe_2O_3 [11], α-FeOOH [12], and freshly formed amorphous ferric oxides [13]. The lack of data on the behavior of iron oxide NPs in biological media does not allow the prediction of the degree of accumulation of iron-contained products in the human body.

The purpose of the paper is to show how the dispersion medium and the size of NPs affect the solubility and colloidal properties of iron oxide NPs in the simplest biological solutions.

2. Materials and methods

In the experiments, three engineered hematite NPs with an average surface particle size of 12, 32 nm (Nanografi Co. Ltd., Turkey), and 115 nm (Advanced Powder Technologies LLC, Russia), accordingly marked as Fe_2O_3-12, Fe_2O_3-32, and Fe_2O_3-115 were used. The morphology of the NPs was studied by a transmission electron microscopy (TEM, Jeol JEM-1400 microscope, Jeol, Japan, NUST "MISiS", resolution up to 0.24 nm, accelerating voltage 120 kV, copper grids with an amorphous carbon substrate) and a scanning electron microscopy (SEM, Vega 3 SBN, Tescan, Czech Republic, NUST "MISiS", resolution up to 8 nm, accelerating voltage 30 kV, without spraying any conductive coating). The TEM and SEM images were processed by the pallet method (at least 100 particles and 40 aggregates for each sample were measured) to find a particle size distribution and the average particle size. The specific surface area of the NPs was measured by the method of low-temperature nitrogen adsorption (SorbiPrep, Meta, Russia, TPU Center for Sharing Use "Nanomaterials and Nanotechnologies"). The average surface particle size was calculated from the specific surface measurement data. It was assumed that the particles had a spherical shape [14]. The phase composition was determined by an X-ray phase analysis (XRD, diffractometer 7000S, Shimadzu, Japan, TPU Center for Sharing Use "Nanomaterials and Nanotechnologies", Tomsk, CuK_β irradiation, voltage 40 kV, the current flowing through the tube 30 mA, the speed of the meter was 1.5 degrees/min in the range from 10 to 120 degrees).

The suspensions of the 100 mg/L concentration of NPs were prepared on the base of the simplest pulmonary fluid (SPF, pH = 3.0 ± 0.2, 20 wt% $C_6H_8O_7$, China) and the simplest sweat fluid (SSF, pH = 6.5 ± 0.2, 0.9 wt% NaCl, Grotex LLC, Russia), water solutions mimicking respiratory and skin penetration into the human body [15,16]. The NPs concentration was chosen based on the preliminary study to receive reproducible results of the colloidal study [17]. We used the composition of SPF instead of pulmonary fluid [15] since the degree of nickel NPs dissolution in SPF and in pulmonary fluid reached the same values [18]. The solutions were prepared in distilled water (pH = 6.5 ± 0.6, conductivity 0.2 μS/cm, aqua distillator DE-4 TZMOI, Tyumen Medico, Russia). The weighing was carried out on a scale ALC-210D4 (Acculab, Germany, ±0.0001 g).

The suspensions were aged for 24 h at 25 ± 2 ℃ with periodic 5 min sonication (ultrasonic bath GRAD 28-35, Grade Technology, Russia, power 100 W). The aliquot of 1 mL was periodically taken for colloidal study and 15 mL was centrifuged in a conical closed tube (Centrifuge 5702, Eppendorf, Germany, 4400 rpm, 15 min). The supernatant was carefully poured off the tube, acidified by adding 0.5 mL of 1 M HNO_3, and stored for not more than 72 h. The concentration of iron ions in the supernatant was determined by the change in the light transmission coefficient (T, %) in a colored solution of iron sulfosalicylate (spectrophotometer PD-303 Apel, Japan, 430 nm, cylindrical glass bulb with a diameter of 12 mm). The calibration graph was plotted in the range of iron ion concentrations C = 2–10 mg/L (T, % = 96.02 − 3.2C). The dissolution rate was estimated as the amount of dissolved iron from the powder sample (α, %). The experiment was repeated 3 times.

The colloidal properties of particles (particle size distribution and zeta potential) of suspensions were studied using the method of dynamic light scattering in a U-shaped polystyrene cuvette at 25 ℃ (Zeta sizer Nano ZS laser analyzer, Malvern, USA, NUST "MISIS", He-Ne laser, 4 mW, 633 nm). The obtained quantitative particle size distribution was used to calculate the average particle size (d_{av}).

3. Results

According to the XRD data, the Fe_2O_3-12 and Fe_2O_3-32 NPs were observed to have hematite structure (α-Fe_2O_3) with peaks appearing at 24.2, 33.2; 35.7, 41, and 50 degrees and corresponded to lattice planes indexes (012), (104), (110), (113) and (024), respectively [19]. The Fe_2O_3-115 sample mainly consisted of hematite with residual amounts of Fe_3O_4 (at 45 (400) and 69 (620) [20]) and Fe (at 62 (214) and 64 (300) [21] (Figure 1).

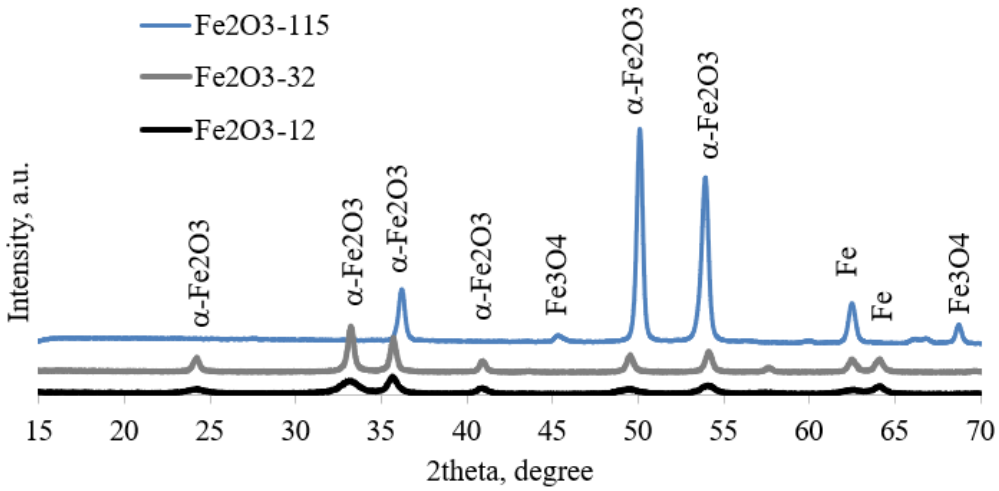

Figure 1. XRD spectra of the particles.

According to TEM and SEM data, the particles were agglomerated (Table 1) and mostly bound by inter-particle (coagulation, not phase) interaction (Figure 2). Fe_2O_3-12 NPs exhibit needle-like morphology (Figure 2a), while bigger NPs have a near-spherical shape (Figure 2b,c).

Table 1. Dispersion and morphology of the studied powders.

Sample	BET	TEM and SEM	
	Specific surface area/Average particle size	Size distribution/average particle (aggregates) size	Shape
Fe_2O_3-12	93.5 m^2/g/12.2 nm	10–119/49.6 nm (64.6–257.7/126 nm)	Needle like
Fe_2O_3-32	35.3 m^2/g/32.4 nm	11.42–57.2/25.6 nm (426–770/570 nm)	Near spherical
Fe_2O_3-115	9.8 m^2/g/114.5 nm	94–492/271 nm (0.9–6.5 μ/2.5 μm)	

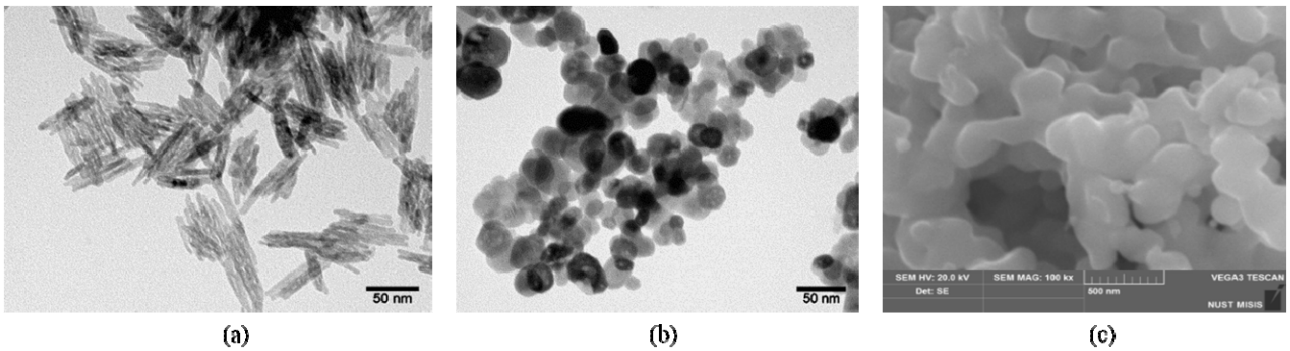

Figure 2. Morphology of (a) Fe_2O_3-12, (b) Fe_2O_3-32 and (c) Fe_2O_3-115 particles.

It was shown that in the selected media, NPs underwent severe agglomeration, which intensified within an hour regardless of the particle size and medium composition (Figure 3) and was

accompanied by the change of the surface charge (Figure 4). After that, the agglomeration reduced, followed by some kind of equilibrium. For example, the average size (d_{av}) of Fe_2O_3-32 agglomerates exposed to the SPF medium for 0.5, 1, 3, and 24 h was 256, 290, 290, and 290 nm, respectively (Figure 3a). Meanwhile, the rate of establishing equilibrium on the surface of the particles was higher in SSF compared to SPF medium: for instance, the rates of charge change (Δξ-change of charge between adjacent measurements) for Fe_2O_3-115 during 3 h were 27 and 36% in SPF (Figure 4a) and SSF media (Figure 4b), respectively. Apparently, the adsorption-desorption processes occurred at the interface of the phases in line with the active dissolution of the surface layer. At further exposure, an equilibrium state was attained on the surface, since the zeta potential of NPs fluctuated within ±1% (Figure 4).

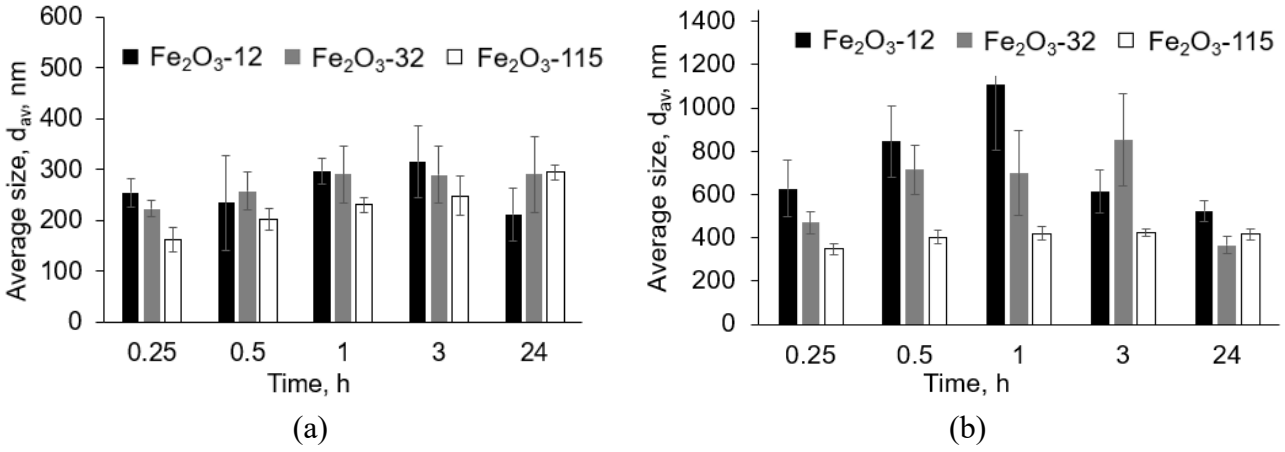

Figure 3. Changes of the average size of aggregates (d_{av}, nm) in (a) SPF and (b) SSF media.

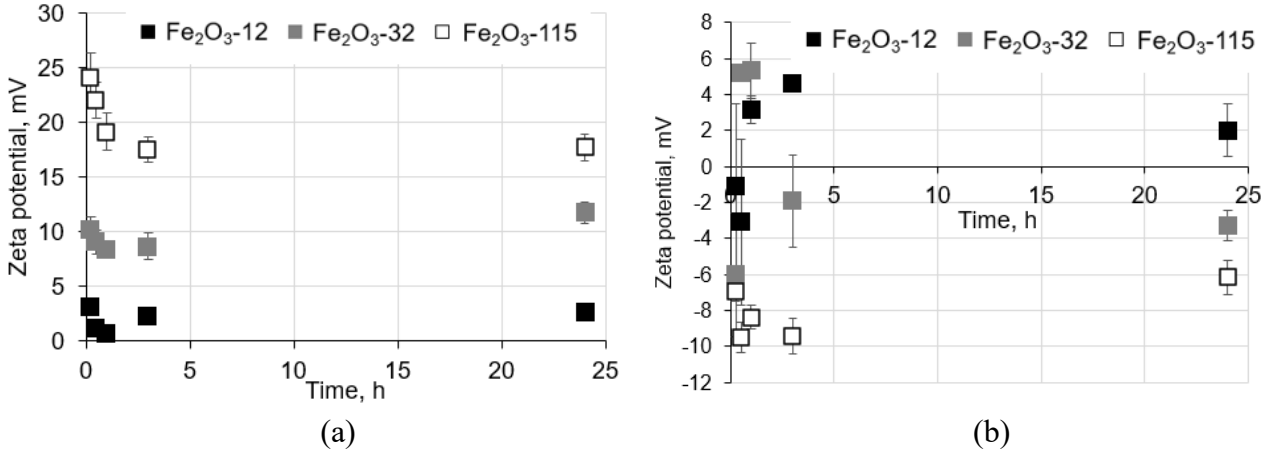

Figure 4. Change of zeta potential of NPs in (a) SPF and (b) SSF media.

It was also observed that the particles were positively charged in SPF at the equilibrium state (≥3 h), while all particles in the SSF except Fe_2O_3-12 had a negative charge. For example, in 3 h zeta potential of Fe_2O_3-32 was +9 and −2 mV in SPF (Figure 4a) and SSF (Figure 4b), respectively. In general, more stable suspensions are formed in the SPF. The more positive charge at lower pH is

proved with DLS measurements of differently sized hematite suspensions (0.5 g/L) in 25 mM NaCl equilibrated for several hours prior to analysis: at pH = 6.5, 8, and 40 nm, NPs had zeta potential of −8 and −26 mV, respectively, while at pH = 3 both particles had of +30 mV zeta potential [22].

It was shown that smaller particles had lower colloidal stability in suspensions. For example, in SPF the equilibrium zeta potential was +2, +9, and +18 mV for the particles with a size of 12, 32, and 115 nm, respectively (Figure 4a). At the same time, the degree of particle agglomeration in fresh (<3 h) suspensions increased in both media with a decrease in the particle size. For example, the d_{av} value was 253, 222, and 166 nm in 15 min SPF solutions for particles with sizes of 12, 32, and 115 nm, respectively (Figure 3a).

Our results about weakening aggregation in acidified medium (SPF, pH = 3) are agreed with the data obtained on α-Fe_2O_3 particles with a size of <50 nm. With the decreasing pH from 6 to 3, the average particle size went down from 611 to 318 nm, and zeta potential increased from +5 to +35 mV in water [14], while hydrodynamic diameter (zeta potential) of 40 nm α-Fe_2O_3 NPs was ~1500 (−35 mV) and ~750 (+30 mV) in 25 mM NaCl, respectively at the pH of 3 and 7 [22].

For bigger Fe_2O_3 particles (<200 nm) pH reduction from 6 to 3 caused the growth of electrophoretic mobility from 3.0 to 3.5 and the size decreased from ~2.3 μm to ~200 nm in water [6]. The charge of both, pristine Fe_3O_4 (51 nm) and citric acid coated Fe_3O_4 particles (58 nm) increased at the pH of 3 compared to 6 [8].

The dissolution study showed that all Fe_2O_3 NPs dissolved in selected solutions: the degree of dissolution (α) reached 1.5% after 15 min (Figure 5). However, the graphs of dissolution degree did not exhibit incremental behavior within 24 h. The curves may be conditionally divided into three stages. Stage 1 is characterized by a rapid increase in the iron concentration in a supernatant. The maximum degree of particle dissolution (α_{max}) is reached in 30 min in SPF (Figure 5a) and after 1 h in SSF (Figure 5b). It can be seen that the dissolution degree in all media for particles with a size <100 nm is greater than for bigger particles: for instance, in SSF α_{max} values are 0.68 and 0.33% for Fe_2O_3-32 and Fe_2O_3-115 particles, respectively (Figure 5b). After reaching the maximum (between 15 and 60 min), the iron content in the supernatant may stay constant (Figure 5a) or decrease (Figure 5b), and a brown precipitate was visually observed mainly in SSF at the stage 2. It was probably iron hydroxide having limited solubility in an aqueous solution. At stage 3, the concentration of iron ions did not change in SSF, although in SPF it increased: α_{max} values were 0.59, 0.31, and 0.23%, respectively, for particles with the size of 12, 32, and 115 nm (Figure 5a).

In general, Fe_2O_3 particles dissolved better in SPF: for example, the dissolution degree of Fe_2O_3-12 NPs after 1 h exposure was 1.29 and 0.78% in SPF and SSF, respectively. A decade ago, it was concluded that reduction of hematite by 10 mM ascorbic acid yielded enhanced rates of Fe(II) production in 25 mM NaCl suspensions of 8 nm α-Fe_2O_3 NPs relative to 40 nm NPs: from pH 2 to 6, reductive dissolution of 8 nm hematite was between 3.3 and 6.5 times faster than 40 nm hematite on the basis of mass [22].

We see that Fe_2O_3 particles dissolve worse than pure 45 nm Fe_3O_4 particles in phosphate-buffered saline after 24 h exposure, where Fe release percentages were between 7 and 12% [23].

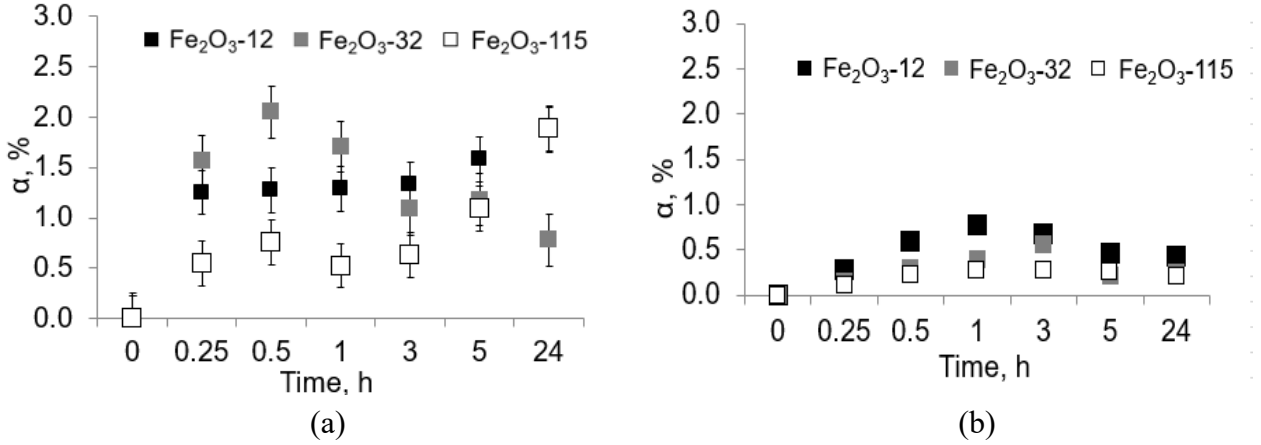

Figure 5. Kinetics of changes in the dissolution degree (α, %) of the particles in (a) SPF and (b) SSF.

Different kinetics of particles dissolution at stage 2 of the dissolution curve in SPF (α did not change for Fe_2O_3-12 and Fe_2O_3-115, while it decreased for the Fe_2O_3-32, Figure 5a) may indicate different dissolution mechanisms. The dissolution of heavy metal oxides may include oxidation or hydrolysis with the formation of hydroxides [24]. The oxidation of iron with an oxidation state of +3 in Fe_2O_3 oxide by O_2 molecules is considered not to be thermodynamically possible. Therefore, we will consider the hydrolysis reaction according to the Eqs 1 and 2:

$$Fe_2O_3 + 3H_2O \rightarrow 2Fe(OH)_3,\ \Delta G_{298} = 51\ kJ/mol \quad (1)$$

$$Fe_2O_3 + 3H_2O \rightarrow 2Fe^{3+} + 6OH^-,\ \Delta G_{298} = 518\ kJ/mol \quad (2)$$

The change in ΔG at 25 °C will be 51 and 518 kJ/mol for the Eqs 1 and 2, respectively [25]. Therefore, it is more likely that the reaction proceeds according to Eq 1. According to the calculated value (ΔG > 0) the Eq 1 cannot proceed at normal conditions. However, it can be assumed that the excess surface energy, so-called "stored energy" (~100 kJ/mol [26]), can be achieved on the surface of particles with a size <100 nm, which may be sufficient to create a barrier.

$Fe(OH)_3$ formed by the Eq 1 has a very low solubility (solubility limit = 6.3×10^{-38} [27]) and should precipitate and, therefore, it would be separated during centrifugation. However, before the formation of the precipitate, the hydroxide is likely to participate via ion exchange after a short time in the solutions: indeed, FeCit is formed in SPF, while $FeCl_3$ is arisen in SSF prior to giving complexes of $[FeCit_6]^{3-}$ and $[FeCl_6]^{3-}$. The precipitation of iron hydroxide was observed visually on the particles at the stage 2 of the dissolution curve (Figure 5). Therefore, the concentration of iron ions in SSF solution did not change after 3 h of holding bigger particles. Nevertheless, available theories cannot explain the accumulated experimental data on the dissolution of iron oxides currently. According to the kinetic and electrochemical regularities of dissolution [28], the process of iron oxide dissolution is determined by the concentration of hydrogen ions and a potential jump that occurs at the oxide/electrolyte interface. The potential of oxide electrodes in slightly acidic media (SSF with pH = 6.5) is determined by the Eq 3:

$$MeO_x + 2xH^+ + 2(x\text{-}0.5z)e = Me^+ + xH_2O \quad (3)$$

The reaction for acidic media (SPF with pH = 3):

$$Me_{n+1}L + e = Me + L \quad (4)$$

where Me—metal, e—electron, MeO—metal oxide, and L—acid anion.

In terms of probability, the accumulation of metal compounds in a body is stipulated by both the penetration of metal-containing particles into the body [29] as well as their subsequent dissolution in the physiological environment [16]. For example, particles with the size of 12, 32, and 115 nm can enter the alveolar region of the lungs (SPF) with a degree (probability P_1) of 50, 43, and 7%, respectively [30], while, the degree of their dissolution (probability P_2) in SPF (after 24 h) is 2.1, 1.4, and 2.3% (Figure 5a). Imagining that NPs penetration into the medium occurs prior to their dissolution, we get that the potential accumulation degree of iron compounds when penetrating with breathing $P_1 \cdot P_2$ maybe 1.05, 0.60, and 0.16%, respectively, for 12, 32, and 115 nm NPs. Thus, the degree of accumulation of iron compounds is obvious to increase with a decrease in inhaled Fe_2O_3 NPs size.

4. Conclusions

This work demonstrated the agglomeration and dissolution behavior of three engineered α-Fe_2O_3 nanoparticles with an average surface particle size of 12, 32, and 115 nm in two physiological solutions—the simplest sweat and pulmonary fluids. Within 60 min exposure, the particle size and concentration of iron released increased in the suspensions, accompanied by an intensive change of the surface charge. After an hour, the colloidal properties did not change significantly, although the degree of dissolution ambiguously fluctuated.

It was shown that the agglomeration of the particles in the simplest pulmonary fluid was lower than in the simplest sweat fluid, compared to the degree of dissolution, which was much higher in the pulmonary fluid than in the sweat. In the simplest pulmonary fluid the colloidal stability of suspensions reduced with a decrease in size of NPs, e.g., the average size of particles was 315, 289, 248 nm, while zeta potential was 2, 9, and 17 mV, respectively for 12, 32, and 115 nm NPs in 3 h suspensions. It was found that 24 h dissolution degree of α-Fe_2O_3 NPs reached 2.33% and 0.41% in the simplest pulmonary and sweat fluids, respectively.

It was assumed that the degree of accumulation of iron compounds increased with the decrease of inhaled Fe_2O_3 NPs size. The mechanism of dissolution of hematite NPs in the slightly acidic and acidic mediums is proposed.

Acknowledgments

The authors express sincere appreciation to Mr. Evgeny Kolesnikov from NUST MISiS for his help with TEM and SEM images. X-Ray and BET analysis was carried out in the framework of Tomsk Polytechnic University Competitiveness Enhancement Program grant, Russia.

Conflict of interest

The authors declare that they have no known competing financial interests or personal relationships that could have appeared to influence the work reported in this paper.

References

1. Dadfar SM, Roemhild K, Drude NI, et al. (2019) Iron oxide nanoparticles: Diagnostic, therapeutic and theranostic applications. *Adv Drug Delivery Rev* 138: 302–325. https://doi.org/10.1016/j.addr.2019.01.005
2. Laurent S, Forge D, Port M (2008) Magnetic iron oxide nanoparticles: synthesis, stabilization, vectorization, physicochemical characterizations, and biological applications. *Chem Rev* 108: 2064–2110. https://doi.org/10.1021/cr068445e
3. Arias LS, Pessan JP, Vieira APM, et al. (2018) Monteiro Iron oxide nanoparticles for biomedical applications: a perspective on synthesis, drugs, antimicrobial activity, and toxicity. *Antibiotics (Basel)* 7: 46. https://doi.org/10.3390/antibiotics7020046
4. Attarad A, Hira Z, Muhammad Z (2016) Synthesis, characterization, applications, and challenges of iron oxide nanoparticles. *Nanotechnol Sci Appl* 9: 49–67. https://doi.org/10.2147/NSA.S99986
5. Roelofs F, Vogelsberger W (2006) Dissolution kinetics of nanodispersed γ-alumina in aqueous solution at different pH: Unusual kinetic size effect and formation of a new phase. *J Colloid Interf Sci* 303: 450–459. https://doi.org/10.1016/j.jcis.2006.08.016
6. Baalousha M (2009) Aggregation and disaggregation of iron oxide nanoparticles: Influence of particle concentration, pH and natural organic matter. *Sci Total Environ* 407: 2093–2101. https://doi.org/10.1016/j.scitotenv.2008.11.022
7. Strehlau JH, Toner BM, Arnold WA, et al. (2017) Accessible reactive surface area and abiotic redox reactivity of iron oxyhydroxides in acidic brines. *Geochim Cosmochim Ac* 197: 345–355. https://doi.org/10.1016/j.gca.2016.10.015
8. Liu J, Dai C, Hu Y (2018) Aqueous aggregation behavior of citric acid coated magnetite nanoparticles: Effects of pH, cations, anions, and humic acid. *Environ Res* 161: 49–60. https://doi.org/10.1016/j.envres.2017.10.045
9. Maenosono S, Suzuki T, Saita S (2007) Mutagenicity of water-soluble FePt nanoparticles in Ames test. *J Toxicol Sci* 32: 575–579. https://doi.org/10.2131/jts.32.575
10. Waite TD, Morel FMM (1984) Photoreductive dissolution of colloidaliron oxide: Effect of citrate. *J Colloid Interf Sci* 102: 121–137. https://doi.org/10.1016/0021-9797(84)90206-6
11. Xu N, Gao Y (2008) Characterization of hematite dissolution affected by oxalate coating, kinetics and pH. *Appl Geochem* 23: 783–793. https://doi.org/10.1016/j.apgeochem.2007.12.026
12. Borer PM, Sulzberger B, Reichar P, et al. (2005) Effect of siderophores on the light-induced dissolution of colloidal iron(III) (hydr)oxides. *Mar Chem* 93: 179–193. https://doi.org/10.1016/j.marchem.2004.08.006
13. Bligh MW, Waite TD (2011) Formation, reactivity, and aging of ferric oxide particles formed from Fe(II) and Fe(III) sources: Implications for iron bioavailability in the marine environment. *Geochim Cosmochim Ac* 75: 7741–7758. https://doi.org/10.1016/j.gca.2011.10.013
14. Godymchuk A, Papina I, Karepina E, et al. (2019) Agglomeration of iron oxide nanoparticles: pH effect is stronger than amino acid acidity. *J Nanopart Res* 21: 208. https://doi.org/10.1007/s11051-019-4634-y
15. Marques MRC, Loebenberg R, Almukainzi M (2011) Simulated biological fluids with possible application in dissolution testing. *Dissolut Technol* 18: 15–28. https://doi.org/10.14227/DT180311P15

16. Midander K, Julander A, Kettelarij J (2016) Testing in artificial sweat—Is less more? Comparison of metal release in two different artificial sweat solutions. *Regul Toxicol Pharm* 81: 381–386. https://doi.org/10.1016/j.yrtph.2016.09.021
17. Langevin D, Raspaud E, Mariot S, et al. (2018) Towards reproducible measurement of nanoparticle size using dynamic light scattering: Important controls and considerations *NanoImpact* 10: 161–167. https://doi.org/10.1016/j.impact.2018.04.002
18. Abzhanova D, Godymchuk A, Gusev A, et al. (2016) Exposure of nano- and ultrafine Ni particles to synthetic biological solutions: predicting fate-related dissolution and accumulation. *EJNM* 8: 203–212. https://doi.org/10.1515/ejnm-2016-0021
19. Zhang YC, Tang JY, Xiao YH (2008) Controllable synthesis and magnetic properties of pure hematite and maghemite nanocrystals from a molecular precursor. *J Alloy Compd* 462: 24–28. https://doi.org/10.1016/j.jallcom.2007.07.115
20. Prakash R, Fanselau K, Mandal TK (2013) A facile synthesis of a carbon-encapsulated Fe_3O_4 nanocomposite and its performance as anode in lithium-ion batteries. *Beilstein J Nanotech* 4: 699–704. https://doi.org/10.3762/bjnano.4.79
21. Mushtaq D (2007) The synthesis of maghemite and hematite (γ-Fe_2O_3, α-Fe_2O_3) nanospheres. *Mater Sci Forum* 534: 157–160. https://doi.org/10.4028/www.scientific.net/MSF.534-536.157
22. Lanzl CA, Baltrusaitis J, Cwiertny DM (2012) Dissolution of hematite nanoparticle aggregates: influence of primary particle size, dissolution mechanism, and solution pH *Langmuir* 28: 15797–15808. https://doi.org/10.1021/la3022497
23. Favela-Camacho SE, Perez-Robles JF, Garcıa-Casillas PE, et al. (2016) Stability of magnetite nanoparticles with different coatings in a simulated blood plasma *J Nanopart Res* 18: 176. https://doi.org/10.1007/s11051-016-3482-2
24. Vodyanitskii YN (2013) Dissolution of magnetite and redistribution of heavy metals in urban soils (model experiment). *Eurasian Soil Sc* 46: 672–680. https://doi.org/10.1134/S1064229313060112
25. Wagman DD, Evans WH, Parker VB, et al. (1989) The NBS tables of chemical thermodynamic properties. Selected values for inorganic and C_1 and C_2 organic substances in SI units. Wanshington, American Society of Chemistry. Available from: https://srd.nist.gov/JPCRD/jpcrdS2Vol11.pdf.
26. Mostovshchikov AV, Ilyin AP, Azanov AA, et al. (2016) The energy stored in the aluminum nanopowder irradiated by electron beam. *Key Eng Mater* 685: 639–642. https://doi.org/10.4028/www.scientific.net/KEM.685.639
27. SenGupta AK (2017) Table of solubility product constants at 25 ℃, *Ion Exchange in Environmental Processes: Fundamentals, Applications and Sustainable Technology*, John Wiley & Sons.
28. Kuzin AV, Gorichev IG, Lainer YA (2013) Stimulating effect of phosphate ions on the dissolution kinetics of iron oxides in an acidic medium. *Russ Metall* 2013: 652–657. https://doi.org/10.1134/S0036029513090073
29. Kreyling W G, Semmler M, Erbe F (2002) Translocation of ultrafine insoluble iridium particles from lung epithelium to extrapulmonary organs is size dependent but very low. *J Toxicol Env Heal A* 166: 998–1004. https://doi.org/10.1080/00984100290071649

30. Oberdörster G, Oberdörster E, Oberdörster J (2005) Nanotoxicology: an emerging discipline evolving from studies of ultrafine particles. *Environ Health Persp* 113: 823–839. https://doi.org/10.1289/ehp.7339

AIMS Press